Soft Matter

PAPER

View Article Online
View Journal | View Issue

Cite this: *Soft Matter*, 2021, **17**, 3096

Alpha helical surfactant-like peptides self-assemble into pH-dependent nanostructures†

Valeria Castelletto, *[a] Jani Seitsonen,[b] Janne Ruokolainen[b] and Ian W. Hamley *[a]

Received 24th November 2020,
Accepted 9th February 2021

DOI: 10.1039/d0sm02095h

rsc.li/soft-matter-journal

A designed surfactant-like peptide is shown, using a combination of cryogenic-transmission electron microscopy and small-angle X-ray scattering, to have remarkable pH-dependent self-assembly properties. Peptide Arg_3-Leu_{12} (R_3L_{12}) forms a network of peptide nanotubes at pH 9 and below. These are associated with α-helical conformation in a "cross-α" nanotube structure, in which peptide dimers lie perpendicular to the nanotube axis, with arginine coated inner and outer nanotube walls. In contrast, this peptide forms decorated vesicular aggregates at higher pH values, close to the pK_a of the arginine residues. These structures are associated with a loss of α-helical order as detected through X-ray scattering, circular dichroism and FTIR spectroscopy, the latter technique also revealing a loss of ordering of leucine side chains. This suggests a proposed model for the decorated or patchy vesicular structures that comprises disordered peptide as the matrix of the membrane, with small domains of ordered peptide dimers forming the minority domains. We ascribe this to a lipid-raft like phase separation process, due to conformational disordering of the leucine hydrophobic chains. The observation of the self-assembly of a simple surfactant-like peptide into these types of nanostructure is remarkable, and peptide R_3L_{12} shows unique pH-dependent morphological and conformational behaviour, with the potential for a range of future applications.

Introduction

Nanotubes formed by the self-assembly of peptides are remarkable anisotropic hollow nanostructures,[1–9] with a diversity of potential applications, for example in biocatalysis,[10–13] encapsulation/release[14–19] and a number of biomedical uses.[20–24] Several distinct architectures of peptide nanotubes have been uncovered, including those based on stacked cyclic peptides with alternating D- and L-residues,[4,25,26] wrapped β-sheet structures,[11,13,27–36] stacked peptide dimer laminate structures,[5,37,38] and coiled coil peptide assemblies.[39–44] Diphenylalanine nanotube structures (with a β-sheet like packing within bilayer walls) have been widely studied, and shown to possess a remarkable range of mechanical, optoelectronic and quantum properties.[45–50]

We have recently reported a novel peptide nanotube architecture, based on α-helical antiparallel peptide dimers of the designed surfactant-like peptide (SLP) R_3L_{12}.[51] These form nanotubes in acidic aqueous solution, in which the peptide dimers lie perpendicular to the tube walls in a so-called "cross-α" nanotube architecture.[51] Tubular network structures were also observed in very acidic solution, at pH 1. These nanotubes present arginine on the inner and outer walls of the nanotubes, which suggests potential uses in antimicrobial or biocatalytic materials.

In comparison to nanotube or nanofibril structures, self-assembled vesicle structures are less commonly observed for peptide systems.[22] Vesicle-like structures have been reported in only a few cases, for example for glycine-rich[52,53] or proline-rich[54] surfactant-like peptides, recombinant amphiphilic peptides[55] and diphenylglycine in aqueous solution[56] or Boc-diphenylalanine [Boc: *tert*-butoxycarbonyl] in HFIP/water.[57]

In the present work, we report the observation of peptide tubular network and compound vesicle structures with decorated surfaces that result from the self-assembly of R_3L_{12} in basic conditions. This peptide contains a dodecameric leucine chain which favours a helical conformation with three arginine residues that impart amphiphilicity, and hence self-assembly properties. Arginine was selected from among the charged amino acids, due to its utility in the future development of antimicrobial systems. In the present paper, we report on the pH-dependent self-assembly of R_3L_{12} at pH values which are tuned by addition of 10 mM NaOH (pH 9), 50 mM NaOH (pH 12) or 100 mM NaOH (pH 13). Concentrations studied

[a] *Department of Chemistry, University of Reading, RG6 6AD, Reading, UK. E-mail: I.W.Hamley@reading.ac.uk*
[b] *Nanomicroscopy Center, Aalto University, Puumiehenkuja 2, FIN-02150 Espoo, Finland*

† Electronic supplementary information (ESI) available: Additional CD spectra, Cryo-TEM and TEM images and SAXS data and SAXS data fitting parameters. See DOI: 10.1039/d0sm02095h

were 0.04 and 0.07 wt% peptide, consistent with our previous work on acidic solutions of R_3L_{12}.[51] The self-assembled nanostructure turns out to be highly pH dependent, and a significant difference is observed between the morphology at pH 9 and pH 12. We additionally examined the behaviour at pH 13 because at pH 12.5 the calculated charge net charge of the peptide changes from +3 to 0 due to deprotonation of the arginine residues as its pK_a is crossed.[9] However, it may be noted that the experimental pK_a may differ in a peptide with multiple charged residues and which undergoes aggregation. Our work reveals a remarkable phase separation process within the membrane of vesicles at high pH which leads to the decoration of the vesicle surface with small domains. Insights from molecular spectroscopies enable this to be associated with the onset of disorder at the molecular level, such that we ascribe the particle formation to phase separation of ordered and disordered domains, reminiscent of lipid rafts.

Experimental

Materials

Peptide R_3L_{12} was supplied by Peptide Protein Research Ltd (Fareham, United Kingdom). The purity was >95% by HPLC using an acetonitrile (0.1% TFA)/water (0.1% TFA) gradient. The molar mass by ESI-MS was 1885.525 g mol^{-1}. Scheme S1 (ESI†) shows the molecular structure of R_3L_{12}, which is capped at both termini.

Sample preparation

Stock solutions of peptide was prepared by dissolving the peptide at 12 (or 22) wt% R_3L_{12} in hexafluoroisopropanol (HFIP), because R_3L_{12} is a highly hydrophobic peptide. An aliquot 1 μl of 12 (or 22) wt% R_3L_{12} in HFIP was added to 15 μl of ultrapure water (ThermoFisher Barnstead) inside a 1.5 ml Eppendorf. The Eppendorf was then vigorously vortexed while adding 2 × 145 μl of ultrapure water, 10 mM NaOH, 47 mM NaOH or 100 mM NaOH to obtain 0.04 (0.07) wt% R_3L_{12} at pH 9, 12 or 13 respectively. The pH was measured with a Mettler Toledo FiveEasy pH meter with Sigma-Aldrich micro pH combination electrode (glass body).

Circular dichroism (CD) spectroscopy

CD spectra were recorded using a Chirascan spectropolarimeter (Applied Photophysics, UK). Peptide solutions were placed in a quartz bottle (1 mm path length). Spectra were measured with a 0.5 nm step, 1 nm bandwidth, and 1 s collection time per step. The CD signal from the water background was subtracted from the CD data of the sample solutions. The absorbance, A, was monitored and presented with $A < 2$ for all data points.

Ellipticity is reported as the mean residue ellipticity ($[\theta]$, in deg cm^2 dmol^{-1}) and calculated as:

$$[\theta] = [\theta]_{obs}\,\mathrm{MRW}(10cl)^{-1} \quad (1)$$

$[\theta]_{obs}$ is the ellipticity measured in millidegrees, MRW is the mean residue molecular weight of the peptide (molecular weight divided by the number of amino acid residues = 15, Scheme S1, ESI†), c is the total concentration in mg ml^{-1}, and l is the optical path length of the cell in cm.

CD spectra were dominated by an α-helical secondary structure. The α-helix content, f_α, is calculated as:[58]

$$f_\alpha = 100[\theta]_{222}/[\theta]_{222,ex} \quad (2)$$

$[\theta]_{222,ex}$ in eqn (2) is the extrapolated value for the molar ellipticity:

$$[\theta]_{222,ex} = [\theta]^{\infty}(1 - k/n) \quad (3)$$

Here $[\theta]_{222,ex} = -29\,608$ deg cm^2 dmol^{-1} because $[\theta]^{\infty} = -37\,400$ deg cm^2 dmol^{-1} is the maximum mean residue ellipticity at 222 nm of a peptide with infinite length and 100% helix content,[58] $n = 12$ is the number of residues/helix (L-residues) and k is a wavelength-dependent constant (2.5 at 222 nm).

Fourier transform infrared spectroscopy (FTIR)

Spectra were recorded using a Thermo Scientific Nicolet iS5 instrument equipped with a DTGS detector, with a Specac Pearl liquid cell (sample contained between fixed CaF_2 plates). Aliquots of peptide at a concentration of 0.04 wt% D_2O with NaOH at specified concentrations, were prepared and added into the liquid cell. Spectra were scanned 128 times over the range 900–4000 cm^{-1}.

Transmission electron microscopy (TEM)

TEM was performed on a JEOL 2100Plus instrument operating at 200 kV. The samples were deposited on copper grids (Agar Scientific, UK) 5.0 mm in diameter and 10 mm thick, coated with carbon film. The samples were stained with 1 wt% uranyl acetate (Sigma-Aldrich, UK), and left to dry at room temperature.

Cryogenic-transmission electron microscopy (cryo-TEM)

Imaging was carried out using a field emission cryo-electron microscope (JEOL JEM-3200FSC), operating at 200 kV. Images were taken in bright field mode and using zero loss energy filtering (omega type) with a slit width of 20 eV. Micrographs were recorded using a Gatan Ultrascan 4000 CCD camera. The specimen temperature was maintained at −187 °C during the imaging. Vitrified specimens were prepared using an automated FEI Vitrobot device using Quantifoil 3.5/1 holey carbon copper grids with a hole size of 3.5 μm. Just prior to use, grids were plasma cleaned using a Gatan Solarus 9500 plasma cleaner and then transferred into the environmental chamber of a FEI Vitrobot at room temperature and 100% humidity. Thereafter 3 μl of sample solution was applied on the grid and it was blotted twice for 5 s and then vitrified in a 1/1 mixture of liquid ethane and propane at temperature of −180 °C. The grids with vitrified sample solution were maintained at liquid nitrogen temperature and then cryo-transferred to the microscope.

The diameter of the nanotubes and the thickness of the nanotube walls were measured from the cryo-TEM images using imageJ software.

Small-angle X-ray scattering (SAXS)

Synchrotron SAXS experiments on solutions were performed on beamline ID02 at the ESRF, Grenoble, France[59] using a flow-through capillary (2 mm internal diameter and wall thickness 0.05 mm) made from borosilicate glass (Hilgenberg GmbH). The radiation damage was carefully checked and the exposure time was limited to one third the value for the onset of damage. The sample was refreshed by displacing the column by 1 μl after each exposure. SAXS images were collected using an EIGER2 detector with a sample-detector distance 0.778 m for the data at high q ($=4\pi \sin\theta/\lambda$ where 2θ is the scattering angle and $\lambda = 1.014$ Å is the X-ray wavelength) and 31 m for the data at low q. The recorded 2D images were checked for isotropy and reduced to one-dimensional intensity profiles. Data reduction was performed as described elsewhere.[59]

Analysis of SAXS data

The SAXS data at pH 9 was fitted using an analytical expression for a form factor describing a cylindrical shell[60] using the software SASfit.[61] The fitting parameters for the cylindrical shell form factor are the core radius, R_c, the shell thickness, D_c, and the scattering length density of the core, η_c, shell, η_s, and solvent, η_{solv}. The SAXS data at pH 12 and pH 13 was fitted using the analytical expression for a system of spherical shells.[60] The parameters for the spherical shell form factor were scale factor, N_s, external shell radius, R_s, shell thickness, D_s, scattering length density of the core, η_c, and shell, η_s. The background was fitted using the expression $a_1 + a_2 q^{-c0}$ where a_1, a_2 and c_0 are constants.

Results

We first probed the conformation of the peptide in the basic aqueous solutions. Circular dichroism (CD) spectra shown in Fig. 1, measured for 0.04 wt% R_3L_{12}, confirm the formation of α-helical coiled coil structures for all solution conditions studied. The CD spectra for 0.07 wt% solutions shown in Fig. S1 (ESI†) also confirm α-helix structure.[62] For 0.04 wt% R_3L_{12}, the α-helical content f_α is, respectively 76%, 34% and 19% at pH 9, 12 and 13.

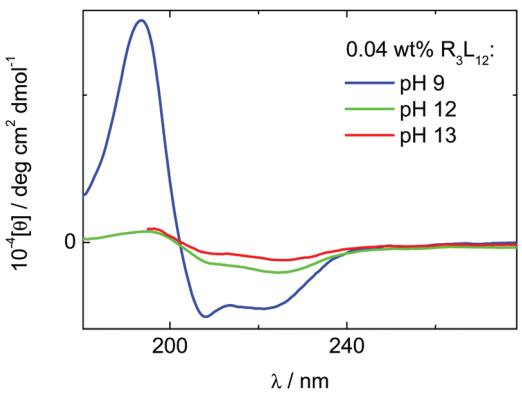

Fig. 1 CD spectra (mean residue ellipticity) for 0.04 wt% R_3L_{12} measured at pH 9, 12 and 13.

For 0.07 wt% R_3L_{12}, the α-helical content f_α is, respectively, 98%, 43% and 20% at pH 9, 12 and 13. The CD spectra therefore indicate a high α-helical content at pH 9, but a substantial loss of this conformation at higher pH. This turns out to significantly affect the self-assembled nanostructure, which we then elucidated using the powerful combination of cryogenic-TEM (TEM: transmission electron microscopy), TEM and SAXS (small-angle X-ray scattering).

Fig. 2 shows representative cryo-TEM images revealing branched nanotubes in a 0.04 wt% solution of R_3L_{12} at pH 9. The nanotube wall thickness measured from the cryo-TEM images was ~3 nm. The nanotube diameter was (16.4 ± 1.7) nm, as calculated from the average of the values plotted in the histogram in the inset in Fig. 2c. These branched nanotubes are very similar to those previously reported by us for 0.04 wt% R_3L_{12} at pH 1,[51] which we proposed are built from α-helical antiparallel peptide dimers arranged perpendicular to the nanotube wall. The branching is believed to result from the increased energetic penalty of charged residues at nanotube ends at low pH. Increasing the concentration to 0.07 wt% R_3L_{12} at pH 9, the α-helical secondary structure is retained as confirmed by CD (Fig. S1, ESI†), but the self-assembly of the peptide into branched nanotubes is disrupted, leading to the coexistence of a nanotube network with more loosely folded peptide sheet-like structures as revealed in the cryo-TEM images in Fig. S2 (ESI†).

SAXS was used to probe the nanostructure in more detail *via* measurements on solutions in basic aqueous solutions at the same concentrations used to prepare samples for cryo-TEM. The SAXS curves measured at pH 9, 12 and 13 for 0.04 and 0.07 wt% R_3L_{12} are displayed in Fig. 3 and Fig. S3 (ESI†) respectively. The SAXS data provide form factors which yield information on the self-assembled nanostructure *in situ* in solution. The fit parameters are listed in Table S1 (ESI†). The data at pH 9 show well-defined oscillations, which result from interference scattering from the nanotube walls, and these features were fitted to a model of a hollow cylinder (long cylindrical shell) consistent with a nanotube structure (also revealed by cryo-TEM, Fig. 2). The nanotube scattering oscillations are superposed on a background which is due to scattering from small clusters visible in the cryo-TEM images and/or unassociated peptides. The SAXS data for the samples at pH 12 and pH 13 show distinct features, with a power-law scattering at low q, which is due to the presence of fractal-like structures, also revealed by cryo-TEM and TEM, to be discussed shortly. The SAXS data was measured out to high q, in order to probe possible peptide secondary structure. A peak corresponding to a spacing $d = 11.2$ Å is apparent in the data in Fig. 3 for the peptide at pH 9 (and at $d = 11.0$ Å at pH 7). This is consistent with the expected diameter of a α-helix.[63,64] This peak is lost at higher pH, consistent with the loss of α-helix secondary structure revealed in the CD spectra in Fig. 1 and also *via* FTIR spectra, to be discussed shortly.

Structural parameters obtained from the SAXS fitting for 0.04 wt% peptide solution at pH 9 provide a nanotube diameter equal to $2 \times [(5.3 + 3.7) \pm 2.8] = 18 \pm 5.6$ nm, which compares

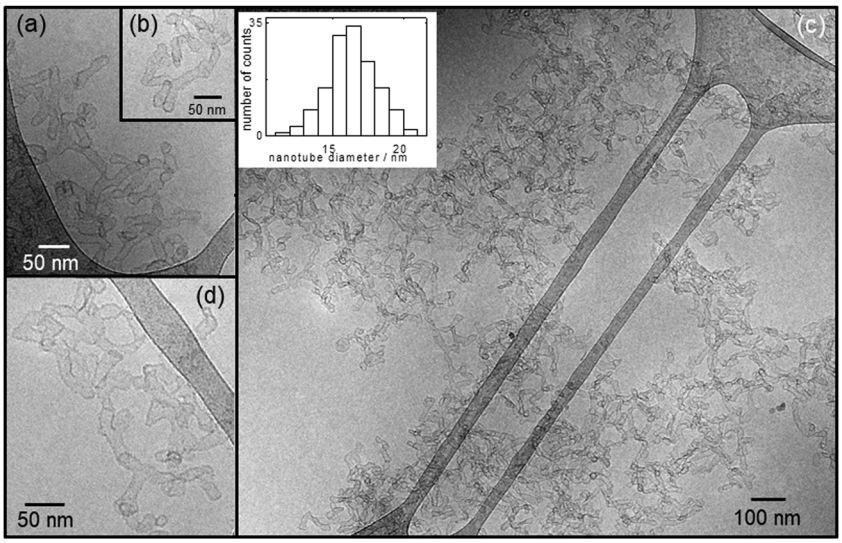

Fig. 2 (a–d) Cryo-TEM images for the branched nanotubes observed at 0.04 wt% R_3L_{12} at pH 9. The inset in (c) shows the distribution of nanotube diameters measured from all the cryo-TEM images.

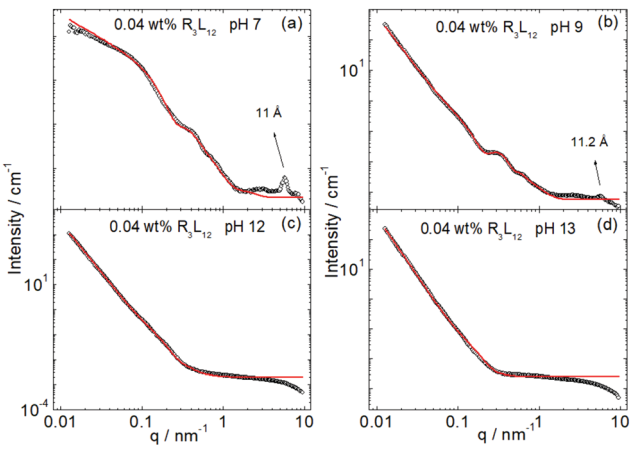

Fig. 3 Measured SAXS intensity profiles (open symbols) fitted with form factors (solid lines) corresponding to nanotubes at pH 7 and pH 9, and spherical shells at pH 12 and pH 13 with a fractal-like background scattering term at pH 9, 12 and 13 only.

very well with 16.4 ± 1.7 nm calculated from the average of the nanotube diameters plotted in Fig. 2c. As previously discussed by us, the nanotube wall thickness corresponds closely to the length of R_3L_{12} estimated using average residue spacings,[64] $l = (0.15n) + (0.34p) = 2.82$ nm (~3 nm) where $n = 12$ (number of L residues in the α-helix) and $p = 3$ (number of R residues). Our results are in agreement with a model for the nanotubes that have walls built from a single layer of α-helical antiparallel peptide dimers.

Increasing the pH from 9 to pH 12 and 13 at 0.04 wt% R_3L_{12}, leads to the self-assembly of the peptide α-helices into globular structures, decorated by well-defined particles (ascribed as phase-separated domains, see below). Cryo-TEM images shown in Fig. 4, Fig. S4 (ESI†) (0.04 wt% R_3L_{12} at pH 12) and Fig. 5 (0.04 wt% R_3L_{12} at pH 13) display several representative examples of cryo-TEM images obtained for such globular structures, along with the cross-section profiles of the image contrast from boxes selected to contain particles decorating the globular structures. Fig. 4f and 5d show histograms for aggregate sizes measured from all the cryo-TEM images. Values averaged over the histograms in Fig. 4f and 5d show that the average size of the globular structures is (23.8 ± 5.9) nm at pH 12 and (29.8 ± 7.6) nm at pH 13 respectively. The globular structures become slightly elongated at pH 13 (Fig. 5). Fig. 4d, e and Fig. 5c show the plots of the contrast averaged within a rectangular box enclosing particles decorating the surface of the globular aggregates. All the profiles are consistent with particles that are 3 nm in width. TEM was used to support the results from Fig. 4 and Fig. S4 (ESI†). Representative TEM results obtained for at 0.04 wt% R_3L_{12} at pH 12 are displayed in Fig. S5 (ESI†). The images show the self-assembly of the α-helices into spherical aggregates, (54.4 ± 14.9) nm, decorated with 3 nm width particles. Additional cryo-TEM images for more concentrated samples (0.07 wt% R_3L_{12}) at pH 12 and 13 are displayed in Fig. S6 and S7 (ESI†) respectively. These reveal particle-decorated globular particle structures as for the 0.04 wt% samples. The size of the phase separated domains obtained from cross-sections of the cryo-TEM images is 3.2–3.7 nm (Fig. S6 and S7, ESI†), with an overall vesicle size in the range 20–40 nm (histogram shown in Fig. S7, ESI†). The vesicle size is consistent with the parameters from the core–shell sphere modelling of the SAXS form factor (Table S1, ESI†).

The cryo-TEM images in Fig. S7a–c (ESI†) for a 0.07 wt% solution show that the peptide self-assembles into somewhat elongated globular structures similar to those discussed above for 0.04 wt% R_3L_{12} at pH 13 (Fig. 5). The size of such globules, averaged over the values plotted in Fig. S7e (ESI†) is (27.5 ± 6.0) nm. Fig. S7d (ESI†) shows the plots of the contrast profile averaged within boxes enclosing particles decorating the surface of the globular particles in Fig. S7a

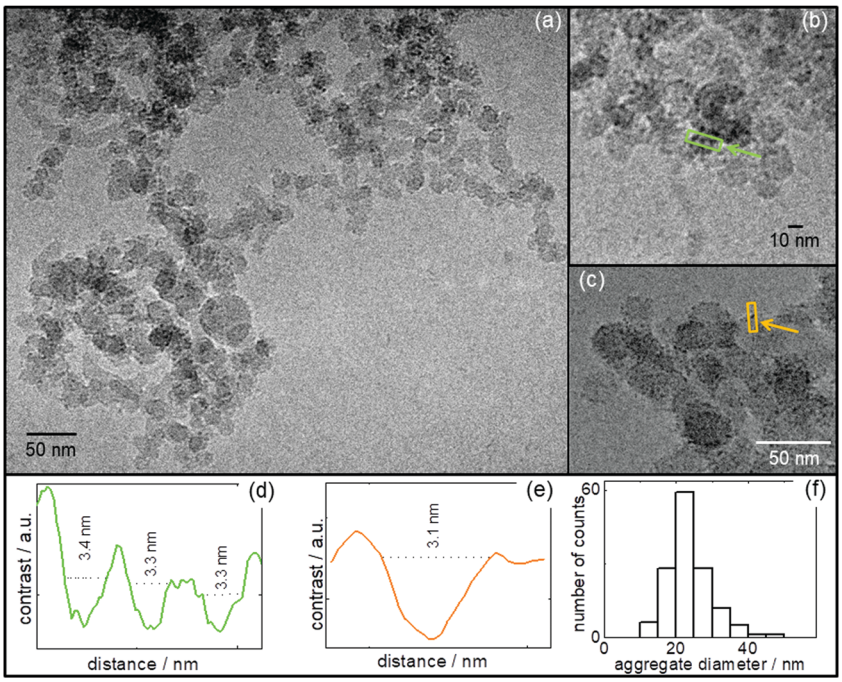

Fig. 4 (a–c) Cryo-TEM images for 0.04 wt% R_3L_{12} at pH 12; (d and e) line contrast profiles from the rectangular masks enclosing particles, as indicated by arrows in (b and c). The colours of boxes in (b and c) correspond to the same colour plots for contrast profiles in (d and e). (f) Size distribution of aggregates, measured from the whole set of cryo-TEM images. The relative contrast scales in (d and e) extend from dark (lower) to light (upper).

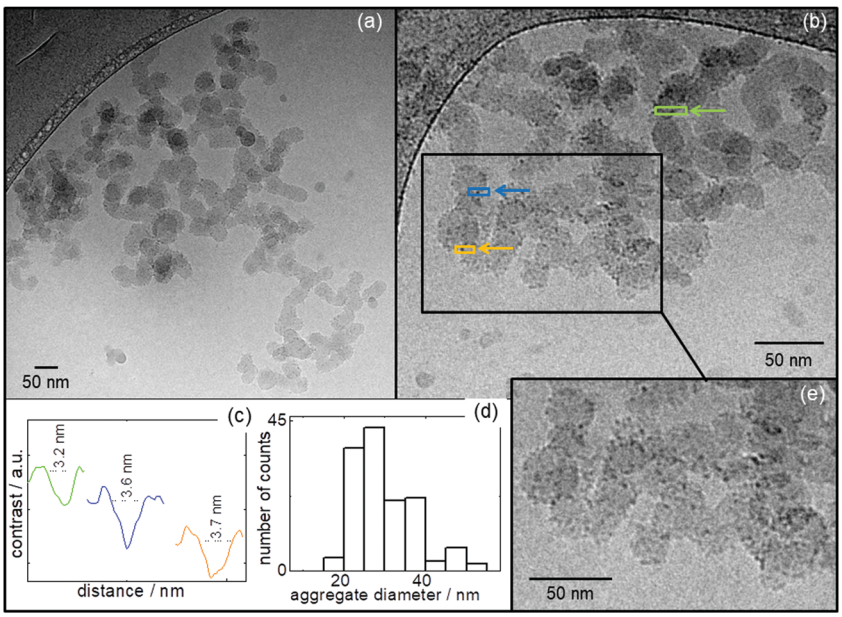

Fig. 5 (a, b and e) Cryo-TEM images for 0.04 wt% R_3L_{12} at pH 13; (c) contrast profiles from rectangular mask enclosing particles, as indicated in (b). The colours of boxes in (b) correspond to the same colour plots of contrast profiles in (c), (d) size distribution of aggregates, measured from the whole set of cryo-TEM images, (e) magnification of area inside the square in (b). The relative contrast scale in (c) extends from dark (lower) to light (upper).

(ESI†). This reveals that the vesicles are decorated with 3 nm-size particles.

The observed particle formation within the vesicle membrane suggests a phase separation process, reminiscent perhaps of lipid raft formation with coexisting domains of less ordered and more ordered peptides. In order to obtain molecular level information on the origin of such structures, we turned to FTIR spectroscopy to probe the ordering within the R_3L_{12} chains, including side chain and hydrogen bond ordering. FTIR spectra for samples at 0.04 and 0.07 wt% are shown in Fig. 6 and Fig. S8

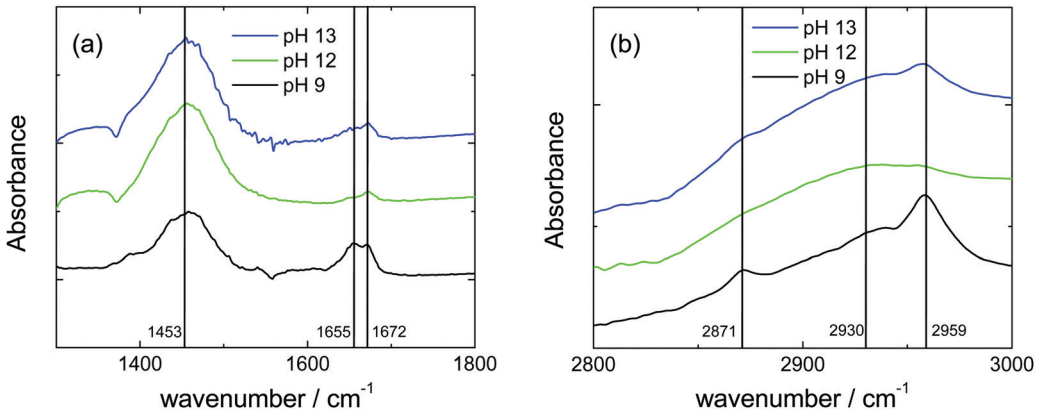

Fig. 6 FTIR spectra for 0.04 wt% solutions of R_3L_{12} at the pH values indicated, in regions of the spectra corresponding to (a) amide I, (b) $CH/CH_2/CH_3$ deformation modes. The positions of main peaks are delineated. Spectra are offset vertically for clarity.

(ESI†) respectively. In the amide A/amide III region the spectra show a large peak near 1453 cm^{-1}, due to N–H stretch modes.[9,65] In the amide I range, sensitive to peptide conformation, the peak at 1655 cm^{-1} is consistent with the α-helical conformation also revealed in the CD spectra (Fig. 1).[9,65,66] An additional peak at 1672 cm^{-1} is mainly due to TFA counterions bound to the peptide.[67–69] The peak due to α-helical conformation is greatly reduced in intensity at pH 12 and pH 13, *i.e.* in the vicinity of the isoelectric point.

Additional valuable insights are provided by the FTIR spectra in the region sensitive to CH_2/CH_3 stretching vibrations, around 2800–2960 cm^{-1}. The spectra shown in Fig. 6 and Fig. S8 (ESI†) contain a broad band centred around 2930 cm^{-1} due to CH/CH_2 stretching modes.[70,71] More prominent are peaks at 2871 and 2959 cm^{-1} which can be assigned to CH_3 end group symmetric and asymmetric stretch vibrations respectively.[70,71] Considering the molecular structure of R_3L_{12}, (Scheme S1, ESI†) these can be assigned to vibrations of the leucine side chain methyl groups. Remarkably, these peaks are much weaker in spectra measured at pH 12 and pH 13, *i.e.* close to the isoelectric point. This, along with the loss of the α-helical FTIR peak (and consistent with CD spectra and the loss of the 11 Å α-helix peak in the SAXS data, Fig. 3) suggests that at this pH, a significant fraction of peptides are present in a disordered conformation. We associate this with the majority of the structure within the vesicle membranes. We propose that the observed small particles decorating the vesicles are associated with small ordered peptide domains, since the cryo-TEM indicates that these domains are approximately on a size scale that corresponds to the length of the molecule in an ordered α-helical conformation. We thus tentatively associate these domains with small clusters of R_3L_{12} dimers.

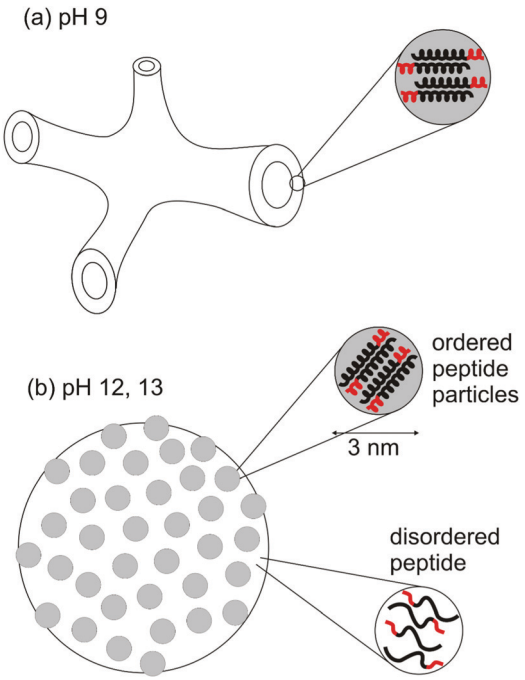

Scheme 1 Schematic summarizing proposed models for ordered and phase separated morphologies observed at different pH values. (a) Nanotube network at pH 9, showing nanotube wall built from R_3L_{12} dimers, wall thickness ~ molecular length, (b) phase-separated vesicle membranes with ordered particles within matrix comprising conformationally disordered peptides.

Discussion and conclusions

We summarize proposed models based on our observations in Scheme 1. Networks of nanotubes are formed at pH 9, as clearly revealed by cryo-TEM. The nanotube walls comprise opposed dimers of α-helices oriented perpendicular to the long axis of the nanotube in the network forming a unique "cross-α" nanotube structure. The peptide charge is +3 at pH 9 and thus the nanotubular network structures are coated with charged arginine residues on the inner and outer surfaces. The α-helices are presumably paired in an opposed configuration to minimize the electrostatic repulsion between arginine residues, as well as maximizing the regular packing of hydrophobic leucine residues. The formation of the tubular network structure as opposed to (open-ended) nanotubes, is ascribed to the unfavorable electrostatic penalty that would result from charges at the ends of uncapped nanotubes.

A very different morphology to a nanotube network is observed near the pK_a of the arginine residues (pK_a = 12–13 expected), comprising hollow globular structures decorated with small particles. Based on the loss of α-helical conformation detected in SAXS profiles and CD and FTIR spectra, we ascribe this structure to a phase separated structure with the majority of the system comprising unordered peptide with significant disorder in the leucine hydrophobic chains (detected by FTIR). The unordered "matrix" coexists with small domains (*ca.* 3 nm in diameter, *i.e.* corresponding to the length of a peptide dimer) comprising phase separated regions of ordered peptide. The unordered peptide domains presumably comprise uncharged peptides due to the loss of the arginine charge at the pK_a, a small fraction of peptide that is still charged may form the minority domains. The phase separation resembles that of lipids associated with formation of lipid rafts, however in the case of R_3L_{12}, the transition from ordered to disordered conformation of the leucine residues coupled to the change in the charge on the arginine residues (loss of charge as pH is increased to the pK_a value) is likely to be the driving force for the proposed phase separation process. In other words, we propose that the presence of coexisting ordered and disordered leucine hydrophobic chains, rather than lipid chains, that may be at the origin of the phase separation.

Phase separated structures within lipid membranes, called lipid rafts, are well known[72–74] and "raspberry" morphology systems comprising agglomerated particles have also been observed for casein (milk protein) micelles[75,76] (so-called) and phase-separating triblock copolymer particles in solution.[77] However, in our case the decorated globular particles are hollow (as revealed by SAXS) and so we do not refer to them as raspberry structures. We are not aware of prior reports on this type of morphology or phase separation process in a purely peptidic system and here we suggest that this process is due to conformational disordering of leucine side chains brought about by pH-dependent changes in electrostatic interactions of the attached arginine residues.

In summary, peptide R_3L_{12} forms a remarkable range of nanostructures, dependent on pH. In our recent Communication, we showed that it forms nanotubes (at pH 2–4) or nanotubular networks (at pH 1) in acidic aqueous solutions.[51] Here we show that nanotube network structures are formed at pH 7 and pH 9, and we present new data showing the α-helical conformation of the peptide in the nanotubes, for the first time from synchrotron SAXS with an extended q range covering the spacing associated with α-helical structures, as well as CD and FTIR spectroscopy. This provides a unique combination of structural and spectroscopic probes of the α-helical structure. At pH values close to the pK_a of the arginine residues (expected pK_a = 12-13), particle-decorated vesicles (or "patchy vesicles") are formed.

It is remarkable that a simple SLP R_3L_{12} forms nanotubes, this being very distinct from the formation of nanotubes from coiled coil aggregation of other α-helical peptides with significantly longer and more complex sequences such as designed heptad repeats.[39–41,43,44,78] In these structures, the nanotube is usually formed from the presence of a hollow core within aggregates of parallel (or somewhat offset) coiled coils. However, nanotubes have been reported for other surfactant-like peptides including A_6K[79–81] and A_6R,[31] although in this case they are based on β-sheet structures and, to the best of our knowledge, R_3L_{12} is only SLP reported to date to have an α-helical nanotube structure. The arginine-coated nanotube network and decorated vesicle nanostructures formed by R_3L_{12} may have a range of valuable applications in biocatalysis, antimicrobial material development or targeted delivery, among others.

Conflicts of interest

There are no conflicts to declare.

Acknowledgements

The work of IWH and VC was supported by EPSRC Platform grant EP/L020599/1. We thank the ESRF for the award of beamtime for SAXS on ID02 (ref. SC-4981) and Thomas Zinn and Theyencheri Narayanan for performing the measurements.

References

1 X. Gao and H. Matsui, *Adv. Mater.*, 2005, **17**, 2037–2050.
2 T. Shimizu, M. Masuda and H. Minamikawa, *Chem. Rev.*, 2005, **105**, 1401–1443.
3 S. Scanlon and A. Aggeli, *Nano Today*, 2008, **3**, 22–30.
4 R. J. Brea, C. Reiriz and J. R. Granja, *Chem. Soc. Rev.*, 2010, **39**, 1448–1456.
5 C. Valéry, F. Artzner and M. Paternostre, *Soft Matter*, 2011, **7**, 9583–9594.
6 R. Chapman, M. Danial, M. L. Koh, K. A. Jolliffe and S. Perrier, *Chem. Soc. Rev.*, 2012, **41**, 6023–6041.
7 I. W. Hamley, *Angew. Chem., Int. Ed.*, 2014, **53**, 6866–6881.
8 T. Shimizu, W. X. Ding and N. Kameta, *Chem. Rev.*, 2020, **120**, 2347–2407.
9 I. W. Hamley, *Introduction to Peptide Science*, Wiley, Chichester, 2020.
10 Z. P. Huang, S. W. Guan, Y. G. Wang, G. N. Shi, L. N. Cao, Y. Z. Gao, Z. Y. Dong, J. Y. Xu, Q. Luo and J. Q. Liu, *J. Mater. Chem. B*, 2013, **1**, 2297–2304.
11 T. O. Omosun, M. C. Hsieh, W. S. Childers, D. Das, A. K. Mehta, N. R. Anthony, T. Pan, M. A. Grover, K. M. Berland and D. G. Lynn, *Nat. Chem.*, 2017, **9**, 805–809.
12 B. Sarkhel, A. Chatterjee and D. Das, *J. Am. Chem. Soc.*, 2020, **142**, 4098–4103.
13 A. Reja, S. P. Afrose and D. Das, *Angew. Chem., Int. Ed.*, 2020, **59**, 4329–4334.
14 G. von Maltzahn, S. Vauthey, S. Santoso and S. Zhang, *Langmuir*, 2003, **19**, 4332–4337.
15 N. Kameta, H. Minamikawa and M. Masuda, *Soft Matter*, 2011, **7**, 4539–4561.
16 R. F. Silva, D. R. Araujo, E. R. Silva, R. A. Ando and W. A. Alves, *Langmuir*, 2013, **29**, 10205–10212.

17 Q. R. Wang, X. Zhang, J. H. Zheng and D. J. Liu, *RSC Adv.*, 2014, **4**, 25461–25469.
18 M. Nambiar, M. Nepal and J. Chmielewski, *ACS Biomater. Sci. Eng.*, 2019, **5**, 5082–5087.
19 Y. Sun, C. M. Fry, A. Shieh and J. R. Parquette, *Chem. Commun.*, 2020, **56**, 10337–10340.
20 C. X. Chen, F. Pan, S. Z. Zhang, J. Hu, M. W. Cao, J. Wang, H. Xu, X. B. Zhao and J. R. Lu, *Biomacromolecules*, 2010, **11**, 402–411.
21 Y. A. Lin, A. G. Cheetham, P. C. Zhang, Y. C. Ou, Y. G. Li, G. S. Liu, D. Hermida-Merino, I. W. Hamley and H. G. Cui, *ACS Nano*, 2014, **8**, 12690–12700.
22 M. Rad-Malekshahi, L. Lempsink, M. Amidi, W. E. Hennink and E. Mastrobattista, *Bioconjugate Chem.*, 2016, **27**, 3–18.
23 A. Manandhar, K. Chakraborty, P. K. Tang, M. Kang, P. C. Zhang, H. G. Cui and S. M. Loverde, *J. Phys. Chem. B*, 2019, **123**, 10582–10593.
24 W. H. Hsieh and J. Liaw, *J. Food Drug Anal.*, 2019, **27**, 32–47.
25 M. R. Ghadiri, J. R. Granja and L. K. Buehler, *Nature*, 1994, **369**, 301–304.
26 J. D. Hartgerink, J. R. Granja, R. A. Milligan and M. R. Ghadiri, *J. Am. Chem. Soc.*, 1996, **118**, 43–50.
27 K. Lu, J. Jacob, P. Thiyagarajan, V. P. Conticello and D. G. Lynn, *J. Am. Chem. Soc.*, 2003, **125**, 6391–6393.
28 M. J. Krysmann, V. Castelletto, J. M. E. McKendrick, I. W. Hamley, C. Stain, P. J. F. Harris and S. M. King, *Langmuir*, 2008, **24**, 8158–8162.
29 A. K. Mehta, K. Lu, W. S. Childers, S. Liang, J. Dong, J. P. Snyder, S. V. Pingali, P. Thiyagarajan and D. G. Lynn, *J. Am. Chem. Soc.*, 2008, **130**, 9829–9835.
30 I. W. Hamley, A. Dehsorkhi, V. Castelletto, S. Furzeland, D. Atkins, J. Seitsonen and J. Ruokolainen, *Soft Matter*, 2013, **9**, 9290–9293.
31 I. W. Hamley, A. Dehsorkhi and V. Castelletto, *Chem. Commun.*, 2013, **49**, 1850–1852.
32 K. L. Morris, S. Zibaee, L. Chen, M. Goedert, P. Sikorski and L. C. Serpell, *Angew. Chem., Int. Ed.*, 2013, **52**, 2279–2283.
33 J. Madine, V. Castelletto, I. W. Hamley and D. A. Middleton, *Angew. Chem., Int. Ed.*, 2013, **52**, 10537–10540.
34 M. H. Koc, G. C. Ciftci, S. Baday, V. Castelletto, I. W. Hamley and M. O. Guler, *Langmuir*, 2017, **33**, 7947–7956.
35 A. Chatterjee, S. P. Afrose, S. Ahmed, A. Venugopal and D. Das, *Chem. Commun.*, 2020, **56**, 7869–7872.
36 J. Li, J. Q. Wang, Y. R. Zhao, P. Zhou, J. Carter, Z. Y. Li, T. A. Waigh, J. R. Lu and H. Xu, *Coord. Chem. Rev.*, 2020, **421**, 15.
37 C. Valery, M. Paternostre, B. Robert, T. Gulik-Krzywicki, T. Narayanan, J. C. Dedieu, G. Keller, M. L. Torres, R. Cherif-Cheikh, P. Calvo and F. Artzner, *Proc. Natl. Acad. Sci. U. S. A.*, 2003, **100**, 10258–10262.
38 C. Tarabout, S. Roux, F. Gobeaux, N. Fay, E. Pouget, C. Meriadec, M. Ligeti, D. Thomas, M. Ijsselstijn, F. Besselievre, D. A. Buisson, J. M. Verbavatz, M. Petitjean, C. Valery, L. Perrin, B. Rousseau, F. Artzner, M. Paternostre and J. C. Cintrat, *Proc. Natl. Acad. Sci. U. S. A.*, 2011, **108**, 7679–7684.
39 M. J. Pandya, G. M. Spooner, M. Sunde, J. R. Thorpe, A. Rodger and D. N. Woolfson, *Biochemistry*, 2000, **39**, 8728–8734.
40 D. N. Woolfson, *Adv. Protein Chem.*, 2005, **70**, 79–112.
41 C. F. Xu, R. Liu, A. K. Mehta, R. C. Guerrero-Ferreira, E. R. Wright, S. Dunin-Horkawicz, K. Morris, L. C. Serpell, X. B. Zuo, J. S. Wall and V. P. Conticello, *J. Am. Chem. Soc.*, 2013, **135**, 15565–15578.
42 N. C. Burgess, T. H. Sharp, F. Thomas, C. W. Wood, A. R. Thomson, N. R. Zaccai, R. L. Brady, L. C. Serpell and D. N. Woolfson, *J. Am. Chem. Soc.*, 2015, **137**, 10554–10562.
43 Y. Y. Wu, P. K. Norberg, E. A. Reap, K. L. Congdon, C. N. Fries, S. H. Kelly, J. H. Sampson, V. P. Conticello and J. H. Collier, *ACS Biomater. Sci. Eng.*, 2017, **3**, 3128–3132.
44 Y. Tian, F. B. Polzer, H. V. Zhang, K. L. Kiick, J. G. Saven and D. J. Pochan, *Biomacromolecules*, 2018, **19**, 4286–4298.
45 M. Reches and E. Gazit, *Science*, 2003, **300**, 625–627.
46 L. Adler-Abramovich and E. Gazit, *Chem. Soc. Rev.*, 2014, **43**, 6881–6893.
47 E. Gazit, in *Annual Review of Biochemistry, Vol. 87*, ed. R. D. Kornberg, Annual Reviews, Palo Alto, 2018, pp. 533–553.
48 G. Wei, Z. Q. Su, N. P. Reynolds, P. Arosio, I. W. Hamley, E. Gazit and R. Mezzenga, *Chem. Soc. Rev.*, 2017, **46**, 4661–4708.
49 P. Makam and E. Gazit, *Chem. Soc. Rev.*, 2018, **47**, 3406–3420.
50 P. C. Ke, R. H. Zhou, L. C. Serpell, R. Riek, T. P. J. Knowles, H. A. Lashuel, E. Gazit, I. W. Hamley, T. P. Davis, M. Fandrich, D. E. Otzen, M. R. Chapman, C. M. Dobson, D. S. Eisenberg and R. Mezzenga, *Chem. Soc. Rev.*, 2020, **49**, 5473–5509.
51 V. Castelletto, J. Seitsonen, J. Ruokolainen, C. Piras, R. Cramer, C. J. C. Edwards-Gayle and I. W. Hamley, *Chem. Commun.*, 2020, **56**, 11977–11980.
52 S. Santoso, W. Hwang, H. Hartman and S. Zhang, *Nano Lett.*, 2002, **2**, 687–691.
53 S. Vauthey, S. Santoso, H. Gong, N. Watson and S. Zhang, *Proc. Natl. Acad. Sci. U. S. A.*, 2002, **99**, 5355–5360.
54 C. Felip-Leon, F. Galindo, J. F. Miravet, V. Castelletto and I. W. Hamley, *J. Phys. Chem. B*, 2017, **121**, 7443–7446.
55 A. J. van Hell, C. I. C. A. Costa, F. M. Flesch, M. Sutter, W. Jiskoot, D. J. A. Crommelin, W. E. Hennink and E. Mastrobattista, *Biomacromolecules*, 2007, **8**, 2753–2761.
56 M. Reches and E. Gazit, *Nano Lett.*, 2004, **4**, 581–585.
57 L. Adler-Abramovich and E. Gazit, *J. Pept. Sci.*, 2008, **14**, 217–223.
58 J. Y. Su, R. S. Hodges and C. M. Kay, *Biochemistry*, 1994, **33**, 15501–15510.
59 T. Narayanan, M. Sztucki, P. Van Vaerenbergh, J. Leonardon, J. Gorini, L. Claustre, F. Sever, J. Morse and P. Boesecke, *J. Appl. Crystallogr.*, 2018, **51**, 1511–1524.
60 I. W. Hamley, *Small-Angle Scattering: Theory, Instrumentation, Data and Applications*, Wiley, Chichester, 2021.
61 I. Bressler, J. Kohlbrecher and A. F. Thünemann, *J. Appl. Crystallogr.*, 2015, **48**, 1587–1598.

62 S. M. Kelly, T. J. Jess and N. C. Price, *Biochim. Biophys. Acta*, 2005, **1751**, 119–139.
63 D. Voet and J. G. Voet, *Biochemistry*, John Wiley, New York, 1995.
64 T. E. Creighton, *Proteins. Structures and Molecular Properties*, W.H. Freeman, New York, 1993.
65 B. Stuart, *Biological Applications of Infrared Spectroscopy*, Wiley, Chichester, 1997.
66 A. Barth, *Biochim. Biophys. Acta, Bioenerg.*, 2007, **1767**, 1073–1101.
67 J. T. Pelton and K. R. McLean, *Anal. Biochem.*, 2000, **277**, 167–176.
68 H. Gaussier, H. Morency, M. C. Lavoie and M. Subirade, *Appl. Environ. Microbiol.*, 2002, **68**, 4803–4808.
69 F. Eker, K. Griebenow and R. Schweitzer-Stenner, *Biochemistry*, 2004, **43**, 6893–6898.
70 H. L. Casal and H. H. Mantsch, *Biochim. Biophys. Acta*, 1984, **779**, 381–401.
71 D. G. Cameron, H. L. Casal and H. H. Mantsch, *Biochemistry*, 1980, **19**, 3665–3672.
72 M. Edidin, *Annu. Rev. Biophys. Biomol. Struct.*, 2003, **32**, 257–283.
73 L. J. Pike, *Biochem. J.*, 2004, **378**, 281–292.
74 K. Jacobson, O. G. Mouritsen and R. G. W. Anderson, *Nat. Cell Biol.*, 2007, **9**, 7–14.
75 P. Walstra, *Int. Dairy J.*, 1999, **9**, 189–192.
76 P. X. Qi, *Lait*, 2007, **87**, 363–383.
77 C. J. Mable, N. J. Warren, K. L. Thompson, O. O. Mykhaylyk and S. P. Armes, *Chem. Sci.*, 2015, **6**, 6179–6188.
78 E. H. Egelman, C. Xu, F. DiMaio, E. Magnotti, C. Modlin, X. Yu, E. Wright, D. Baker and V. P. Conticello, *Structure*, 2015, **23**, 280–289.
79 S. Bucak, C. Cenker, I. Nasir, U. Olsson and M. Zackrisson, *Langmuir*, 2009, **25**, 4262–4265.
80 C. C. Cenker, P. H. H. Bomans, H. Friedrich, B. Dedeoglu, V. Aviyente, U. Olsson, N. Sommerdijk and S. Bucak, *Soft Matter*, 2012, **8**, 7463–7470.
81 D. A. Middleton, J. Madine, V. Castelletto and I. W. Hamley, *Angew. Chem., Int. Ed.*, 2013, **52**, 10537–10540.

